Received: 17 July 2023 | Revised: 19 October 2023 | Accepted: 20 October 2023

DOI: 10.1002/nbm.5073

RESEARCH ARTICLE

NMR IN BIOMEDICINE WILEY

Investigating the origin of the ^{13}C lactate signal in the anesthetized healthy rat brain in vivo after hyperpolarized [1-^{13}C]pyruvate injection

Minjie Zhu[1] | Aditya Jhajharia[1] | Sonal Josan[2] | Jae Mo Park[3,4,5] | Yi-Fen Yen[6] | Adolf Pfefferbaum[7] | Ralph E. Hurd[8] | Daniel M. Spielman[8] | Dirk Mayer[1,9]

[1]Department of Diagnostic Radiology and Nuclear Medicine, University of Maryland School of Medicine, Baltimore, Maryland, USA

[2]Digital Health, Siemens Healthineers, Erlangen, Germany

[3]Advanced Imaging Research Center, The University of Texas Southwestern Medical Center, Dallas, Texas, USA

[4]Department of Radiology, The University of Texas Southwestern Medical Center, Dallas, Texas, USA

[5]Department of Biomedical Engineering, The University of Texas Southwestern Medical Center, Dallas, Texas, USA

[6]Martinos Center for Biomedical Imaging, Massachusetts General Hospital, Boston, Massachusetts, USA

[7]Department of Psychiatry and Behavioral Sciences, Stanford University School of Medicine, Stanford, California, USA

[8]Department of Radiology, Stanford University School of Medicine, Stanford, California, USA

[9]Fischell Department of Bioengineering, University of Maryland, College Park, Maryland, USA

Correspondence
Dirk Mayer, Department of Diagnostic Radiology and Nuclear Medicine, University of Maryland School of Medicine, 22 South Greene Street, Baltimore, MD 21201, USA.
Email: dmayer@som.umaryland.edu

Funding information
This work was supported by NIH grants R21 NS096575, R01 DK106395, R21 CA213020, R21 CA202694, R01 EB009070, R01 NS107409, and R21 GM137227. We also acknowledge the support of the University of Maryland, Baltimore, Institute for Clinical & Translational Research (ICTR) and Clinical Translational Science Award (CTSA) grant number 1UL1TR003098.

Abstract

The goal of this study was to investigate the origin of brain lactate (Lac) signal in the healthy anesthetized rat after injection of hyperpolarized (HP) [1-^{13}C]pyruvate (Pyr). Dynamic two-dimensional spiral chemical shift imaging with flow-sensitizing gradients revealed reduction in both vascular and brain Pyr, while no significant dependence on the level of flow suppression was detected for Lac. These results support the hypothesis that the HP metabolites predominantly reside in different compartments in the brain (i.e., Pyr in the blood and Lac in the parenchyma). Data from high-resolution metabolic imaging of [1-^{13}C]Pyr further demonstrated that Lac detected in the brain was not from contributions of vascular signal attributable to partial volume effects. Additionally, metabolite distributions and kinetics measured with dynamic imaging after injection of HP [1-^{13}C]Lac were similar to Pyr data when Pyr was used as the substrate. These data do not support the hypothesis that Lac observed in the brain after Pyr injection was generated in other organs and then transported across the blood–brain barrier (BBB). Together, the presented results provide further evidence that even in healthy anesthetized rats, the transport of HP Pyr across the

Abbreviations used: Ala, alanine; ANOVA, analysis of variance; BBB, blood–brain barrier; Bic, bicarbonate; CSI, chemical shift imaging; EDTA, ethylenediaminetetraacetic acid; ETL, echo train length; FOV, field of view; FSE, fast spin-echo; HP, hyperpolarized; HSD, honestly significant difference; Lac, lactate; MRI, magnetic resonance imaging; MRS, magnetic resonance spectroscopy; NEX, number of excitations; PE, phase encoding; Pyr, pyruvate; RF, radiofrequency; ROI, region of interest; spCSI, spiral chemical shift imaging; SW, spectral width; TE, echo time; TR, repetition time.

BBB is sufficiently fast to permit detection of its metabolic conversion to Lac within the brain.

KEYWORDS
blood–brain barrier, brain metabolism, hyperpolarized ^{13}C, lactate, pyruvate, rat

1 | INTRODUCTION

Metabolic imaging of hyperpolarized (HP) ^{13}C-pyruvate (Pyr) has been applied in multiple rodent studies to investigate brain metabolism in healthy animals[1–6] and disease models such as brain tumor,[7–12] traumatic brain injury,[13–15] and neuroinflammation.[16–18] In these studies, conversion of the injected pyruvate into lactate (Lac) was used to provide information on glycolytic brain metabolism. However, a report by Miller et al.[19] concluded "that earlier reports of whole-brain metabolism in anaesthetized animals may be confounded by partial volume effects and not informative enough for translational studies", after the authors failed to observe HP ^{13}C-lactate in the brain of healthy rats or in normal-appearing brain tissue of animals with brain tumor. The goal of the current study was to further investigate the origin of the lactate signal in the anesthetized rat brain after injection of HP [1-^{13}C]pyruvate. Using a model based on previously reported cerebral transport kinetics, Hurd et al.[2] demonstrated that metabolite kinetics in dynamic metabolic imaging of HP [1-^{13}C]Pyr are consistent with Pyr-to-Lac conversion being limited by blood–brain barrier (BBB) transport. Consequently, Pyr and Lac predominantly would originate from different compartments within the brain (i.e., Pyr in the blood and Lac in the parenchyma). In this study, we used a dynamic two-dimensional (2D) spiral chemical shift imaging (spCSI) sequence that was modified to include a bipolar gradient pulse prior to data acquisition to suppress signal components from flowing spins.[20,21] This approach has been successfully applied in abdominal and cardiac imaging of HP Pyr to suppress the large vascular signal of the injected substrate.[22–24] The method was used to test the hypothesis that signal from brain Lac will be less affected by flow suppression than Pyr. The experiments with flow suppression after HP [1-^{13}C]Pyr injection were complemented by high-resolution metabolic imaging, as well as three-dimensional (3D) metabolic imaging after injection of HP [1-^{13}C]Lac.

2 | EXPERIMENTAL

2.1 | Animal handling and polarization

Six healthy male Wistar rats were included in the experiments. Five rats (240–284 g body weight) received injections of HP [1-^{13}C]Pyr, while the sixth animal (215 g body weight) received an injection of HP [1-^{13}C]Lac. The animals were anesthetized with isoflurane (1.5%–2% in 1–1.5 L/min O_2) during tail vein catheterization and throughout the imaging session. Samples consisting of ~60 mg [1-^{13}C]pyruvic acid and 15 mM trityl radical were hyperpolarized for at least 2.75 h in a 5-T GE SPINLab (Research Circle Technology, Niskayuna, NY, USA), as previously described.[14] The pyruvic acid was then quickly dissolved in water and neutralized with sodium hydroxide to produce a target solution of 125 mM [1-^{13}C]Pyr with pH ~ 7 and a liquid-state polarization at the time of dissolution of 30%–40%.

A 74.4 mg sample of 1.7 M [1-^{13}C]sodium lactate in 37.5:62.5 w/w water: glycerol with 15 mM OX063 and mixed with approximately 7 µL of a 1:50-solution of Dotarem was polarized using a HyperSense system (Oxford Instruments Molecular Biotools, Oxford, UK) operating at 3.35 T and 1.4 K, as previously described.[25] Dissolving the sample with 4 g of 40 mM Tris pH 7.6 containing 100 mg/L disodium ethylenediaminetetraacetic acid (EDTA) produced a final solution of 33 mM lactate with a polarization of approximately 25% at the time of dissolution. Each sample was transferred to the imaging magnet in a syringe within 36 s, and a bolus was injected by hand into the catheterized tail vein followed by a 0.5 mL saline flush. With an injection rate of approximately 0.4 mL/s, each injection plus flush took approximately 9–10 s. The dose for pyruvate and lactate was approximately 1 and 0.4 µmol/g, respectively. All procedures were approved by the respective Institutional Animal Care and Use Committees.

2.2 | MR hardware and acquisition parameters

The experiments with Pyr as the substrate were performed on a clinical 3-T GE 750w MR scanner (GE Healthcare, Waukesha, WI, USA) using a dual-tuned ^{1}H/^{13}C quadrature radiofrequency (RF) coil (50 mm inner diameter; USA Instruments Inc., Aurora, OH, USA) for both excitation and signal reception. The gradient system had a maximum amplitude of 33 mT/m and a slew rate of 120 mT/m/ms. The experiments with Lac as the substrate were performed on a clinical 3-T GE Signa MR scanner (GE Healthcare) equipped with a high-performance insert gradient coil operating at a maximum amplitude of 500 mT/m with a slew rate of 1865 mT/m/ms. The RF coil was of the same design as described above.

To add flow suppression, the existing dynamic 2D spCSI sequence[26] was modified by inserting a bipolar trapezoidal gradient of variable duration 2 W between RF excitation and the spiral readout gradients (Figure S1). In the presence of the bipolar gradient along the *x*-axis, signal from flowing spins (assuming flow velocity in the *x*-axis only) will be attenuated due to the phase accumulation according to the voxel-dependent velocity profile $v(x)$ by a factor

$$\alpha_{sup} = \int_{voxel} \exp(-i\gamma m_1 v(x)) dv. \quad (1)$$

Here, γ is the gyromagnetic ratio and m_1 is the first moment of the bipolar gradient. The amplitude along the *z*-direction of the flow-suppression gradient was 30 mT/m. Because of the pulse sequence implementation, the amplitude along the *x*- and *y*-directions was limited to $\sqrt{0.5}$ times the maximum gradient strength (i.e., 23.3 mT/m). To achieve different levels of flow suppression, each animal was scanned with W of 0, 6, and 9.568 ms (in the following referred to as 9.6 ms) in a randomized order. These durations correspond to first moments (m_1) of 0, 773, and 2025 mT·ms^2/m along the *x*- and *y*-axes, and 0, 995, and 2607 mT·ms^2/m along the *z*-axis, respectively. The corresponding echo times (TEs)—that is, start of the spiral gradients and data acquisition—were 5.296, 16.0, and 23.136 ms. These TEs were chosen so that each dataset included data from 19 spiral gradient echoes, starting at a TE of 23.136 ms. The remaining sequence parameters were: 40 mm field of view (FOV), 2.5×2.5 mm^2 nominal in-plane resolution, eight spatial interleaves, and 280 Hz spectral width (SW). The spiral waveforms were designed using an optimal control theory-based algorithm[27] with the rewinder part calculated using a convex optimization method.[28] For four animals the data were acquired using a constant 5.625° flip angle excitation for 16 datasets every 3 s starting 6 s after the start of the pyruvate injection. For one animal (rat 2), the data acquisition started 9 s after the start of the pyruvate injection, acquiring six datasets every 3 s with a variable flip angle scheme, ending in 90°[29] applied across the total 48 individual excitations. One animal (rat 5) underwent a second magnetic resonance imaging (MRI) session after 1 week to acquire metabolic imaging data at higher resolution without additional flow suppression (36 mm FOV, 24×24 matrix size, 24 spatial interleaves, 24 spiral echoes at a 264 Hz SW, TE = 2.5 ms, 3 s temporal resolution); first injection: 5.625° flip angle, 16 time points starting 15 s after the start of injection; second injection: variable flip angle scheme, three time points starting 24 s after the start of injection. Time-resolved metabolic imaging after the injection of HP lactate was performed using 3D spCSI[30] with the following parameters: FOV = $43.5 \times 43.5 \times 64.8$ mm^3, $16 \times 16 \times 12$ matrix, single spiral interleaf, 32 spiral echoes, SW = 280 Hz, and TE = 2.5 ms. A total of 16 datasets were acquired every 3 s, beginning 9 s after the start of the substrate injection. The variable flip angle scheme ending in a 90° was applied across the total 192 excitations (16 time points, 12 phase-encoding [PE] steps per time point).

In all imaging sessions, single-shot fast spin-echo (FSE) proton MR images were acquired in axial, sagittal, and coronal orientations as anatomical references for prescribing the ^{13}C-CSI experiments. In each direction, up to 13 3 mm slices were acquired with 0 mm separation and a nominal in-plane resolution of 0.47 mm (256×128 matrix, TE/repetition time [TR] = 82/2134 ms). Additionally, ^{1}H multislice 2D axial dual TE ^{1}H-FSE images were obtained for overlay of the metabolic images. The parameters of the overlay scan for the five rats with HP [1-^{13}C]Pyr injection were: 1 mm thickness, 8×8 cm^2 FOV, 256×192 matrix, TR/TE1/TE2 = 3000/41.9/83.7 ms, echo train length (ETL) = 8, and number of excitations (NEX) = 4. For the rat with HP [1-^{13}C]Lac injection, the parameters were: 1.35 mm thickness, 6.4×6.4 cm^2 FOV, 256×256 matrix, TR/TE1/TE2 = 5000/11.3/56.7 ms, ETL = 8, and NEX = 2.

2.3 | Data processing and statistical analysis

The dynamic 2D and 3D spCSI data were reconstructed with custom software written in MATLAB, as described in[26] and,[30] respectively. The spatial k-space dimensions were apodized with a Hanning window and zero-filled by a factor of two, while the temporal dimension was apodized with 15 Hz Gaussian line broadening and zero-filled by a factor of four. Metabolic maps for Pyr, Lac, and alanine (Ala) were calculated by integrating the signal within a 44 Hz interval around each peak in absorption mode. When comparing datasets with different levels of flow suppression, only the k-space data of the 19 echoes starting at a TE of 23.136 ms were used in order to remove differences in T_2 weighting. For each experiment, three regions of interest (ROIs)—brain, vascular, and muscle—were drawn based on the metabolic maps and ^{1}H images. The muscle region was selected based on the anatomical structure corresponding to rat tongue and the observation of alanine signal from the metabolic maps.

The effects of flow suppression were analyzed using a repeated measures analysis of variance (ANOVA) with the Greenhouse–Geisser correction for lack of sphericity. Follow-up between group differences was conducted with Tukey's honestly significant difference (HSD) test. For each dissolution, variations in the level of polarization and concentration of the final solution can affect the absolute signal intensity of pyruvate and its metabolic products, and hence, mask potential effects of flow attenuation. To remove the effect of differences in polarization, the analysis was repeated with each dataset normalized to the respective muscle Ala. Additionally, the same ANOVA was applied to the concentration of the Pyr solution for each injection estimated from the amount of pyruvic acid in the sample vial and the total volume of the final solution. The statistical analysis was performed using the Real Statistics Resource Pack add-in to Microsoft Excel. The investigators were not blinded.

3 | RESULTS

Figure 1A shows the ^{1}H MRI indicating the slice location and position of ROIs in brain, vasculature, and tongue muscle. Metabolic maps of Pyr and Lac with different levels of flow suppression from a representative animal are shown in Figure 1B,C. The metabolic maps for Pyr clearly show the signal decrease in the vascular and, to a lesser degree, brain ROIs with an increasing level of flow suppression. At the same time, no systematic decrease in brain Lac is discernable. The quantitative analysis for both Pyr and Lac from vascular and brain ROIs is shown in Figure 2. Vascular Pyr decreased from 4.0 ± 1.7 (mean ± standard deviation) at W = 0 ms to 2.7 ± 0.6 at W = 6 ms and to 1.6 ± 0.5 at W = 9.6 ms. The ANOVA revealed a statistically significant difference of the Pyr intensity between at least two W values ($F[1.52, 6.08] = 7.13$, $p = 0.0295$). Follow-up tests showed significant differences between W = 0 ms and W = 9.6 ms ($p = 0.0134$). However, only a trend for a similar dependence on flow suppression was found for Pyr in the brain ROI, which decreased from 2.1 ± 1.0 at W = 0 ms to 1.6 ± 0.6 at W = 6 ms and 1.0 ± 0.3 at W = 9.6 ms ($F[1.45, 5.80] = 5.14$, $p = 0.0583$). No significant dependence on the level of flow suppression was detected for Lac in brain (0.5 ± 0.2 at W = 0 ms, 0.4 ± 0.1 at W = 6 ms, 0.4 ± 0.1 at W = 9.6 ms; $F[1.48, 5.93] = 0.32$, $p = 0.6756$) or vascular ROIs (0.43 ± 0.19 at W = 0 ms, 0.33 ± 0.09 at W = 6 ms, 0.22 ± 0.05 at W = 9.6 ms; $F[1.57, 6.29] = 3.8$, $p = 0.0865$). No difference in concentration of the injected Pyr solution was found (122 ± 15 mM at W = 0 ms, 115 ± 12 mM at W = 6 ms, 131 ± 38 mM at W = 9.6 ms; $F[1.42, 5.69] = 0.50$, $p = 0.57$).

Variation in substrate polarization could mask effects on the metabolite signal. Because the SPINlab was designed for clinical applications, it does not provide a reliable measure of polarization for sample volumes as small as those used in this preclinical study. Ala generated in the tongue muscle tissue can be considered stationary compared with signal in blood. Because it did not show any dependence on flow suppression (0.3 ± 0.1 at W = 0 ms, 0.3 ± 0.05 at W = 6 ms, 0.3 ± 0.1 at W = 9.6 ms; $F[1.60, 6.40] = 0.74$, $p = 0.4832$), it was used as a normalization factor to remove the effects of varying polarization. Metabolic maps after normalization to muscle Ala are shown in Figure 3 and the statistical analysis results are shown in Figure 4. In addition to vascular Pyr (12.5 ± 3.3 at W = 0 ms, 8.4 ± 3.1 at W = 6 ms, to 6.1 ± 2.0 at W = 9.6 ms; $F[1.66, 6.64] = 15.86$, $p = 0.0036$), brain Pyr also showed a significant effect of flow suppression (6.9 ± 3.0 at W = 0 ms, 5.2 ± 2.6 at W = 6 ms, to 4.1 ± 1.7 at W = 9.6 ms; $F[1.76, 7.03] = 8.46$, $p = 0.0149$). Follow-up tests showed significant differences between W = 0 ms and W = 6 ms ($p = 0.0181$), as well as between W = 0 ms and W = 9.6 ms ($p = 0.0014$) for vascular Pyr and between W = 0 ms and W = 9.6 ms ($p = 0.0087$)

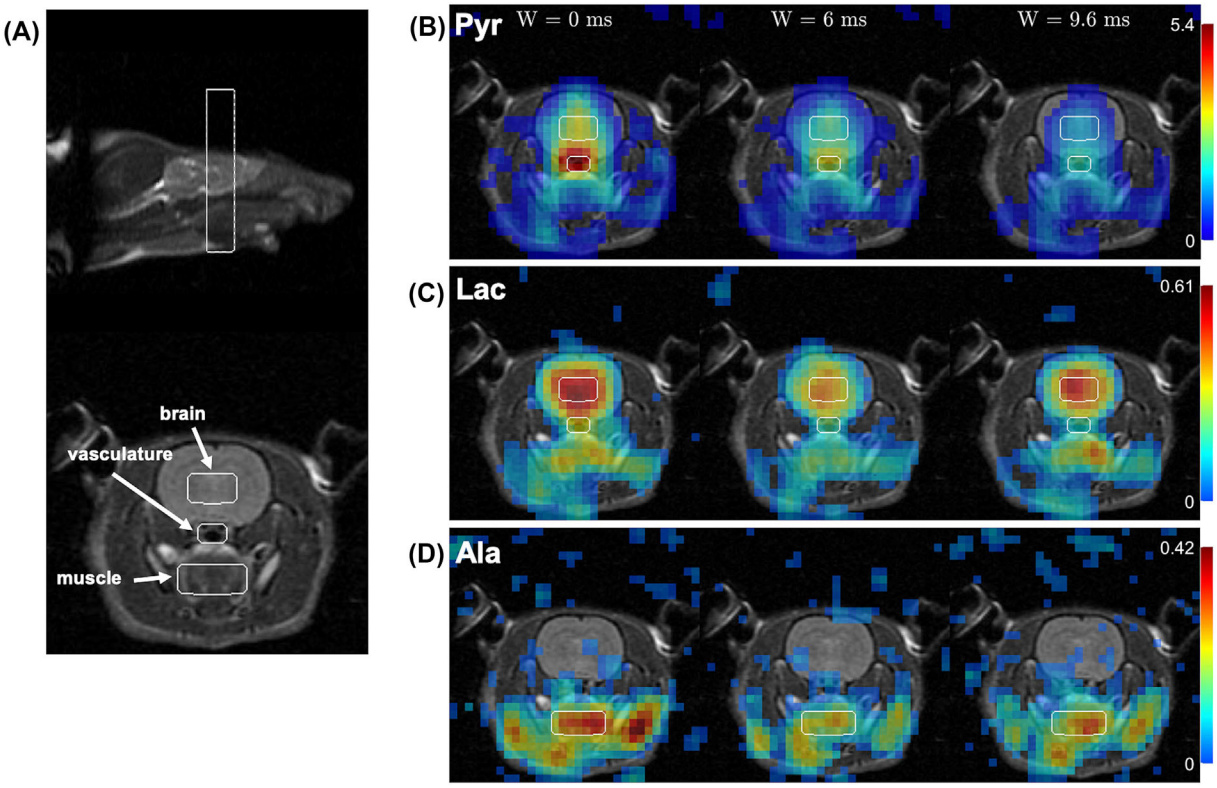

FIGURE 1 ^{1}H MRI and time-averaged metabolic maps at three levels of flow suppression (W = 0, 6, and 9.6 ms) from a representative animal. (A) ^{1}H MRI indicating the slice location and ROIs in brain, vasculature, and tongue muscle. Metabolic maps of (B) Pyr (signal threshold of the metabolic maps 8%), (C) Lac (signal threshold 20%), and (D) Ala (signal threshold 20%). Pyr intensity in the vascular ROI decreased significantly with increasing level of flow suppression. Less variation was observed for brain Lac and muscle Ala. Ala, alanine; Lac, lactate; Pyr, pyruvate; ROI, region of interest.

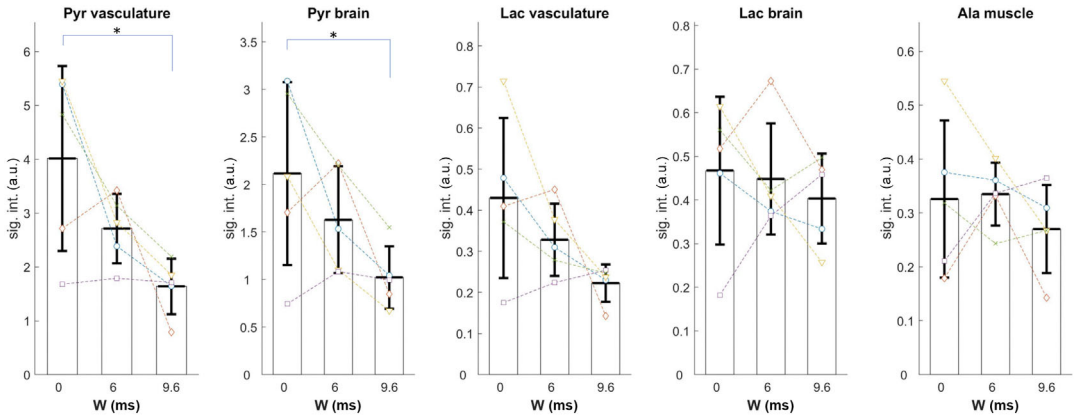

FIGURE 2 Mean and standard deviation ($n = 5$) of time-averaged Pyr, Lac, and Ala in vascular, brain, and muscle ROIs. Signal intensities (sig. int.) are in absolute units (i.e., without any normalization), with each metabolite on the same scale. Data points for each individual animal are shown in dashed lines. Pyr intensity in vasculature and brain was significantly lower with high flow suppression (W = 9.6 ms) compared with no suppression (W = 0 ms). Differences in vascular and brain Lac as well as muscle Ala were not statistically significant for each pair of W values. *$p < 0.05$ for correlated samples. Ala, alanine; Lac, lactate; Pyr, pyruvate; ROI, region of interest.

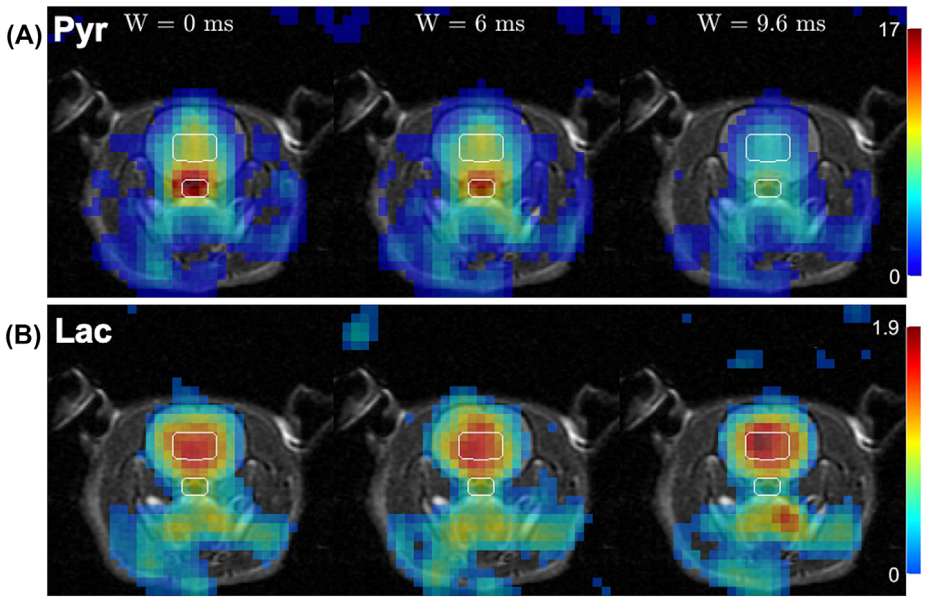

FIGURE 3 Time-averaged metabolic maps for (A) Pyr, and (B) Lac from the animal shown in Figure 1 after normalization to mean Ala intensity in muscle ROI. After normalization, the trend of decreasing vascular Pyr with increasing level of flow suppression was more pronounced, while even less variation in brain lactate can be observed among three levels of suppression. Ala, alanine; Lac, lactate; Pyr, pyruvate; ROI, region of interest.

for brain Pyr. As in the case of absolute metabolite intensities, no significant dependence on the level of flow suppression was detected for brain Lac (1.6 ± 0.8 at W = 0 ms, 1.4 ± 0.5 at W = 6 ms, 1.7 ± 1.0 at W = 9.6 ms; F[1.33, 5.33] = 1.38, $p = 0.31$). Although not statistically significant, a trend of decreasing vascular Lac was observed (1.4 ± 0.5 at W = 0 ms, 1.0 ± 0.3 at W = 6 ms, 0.9 ± 0.1 at W = 9.6 ms; F[1.09, 4.37] = 6.29, $p = 0.0598$).

Metabolic maps of Pyr and Lac, as well as the Lac-to-Pyr ratio acquired at the higher nominal in-plane resolution of 1.5 mm, are shown in Figures 5 and S2. The high-resolution images show clearly different signal distributions for Pyr and Lac. The Pyr maps have the highest intensity in the vascular structures such as the arteries of the Circle of Willis and, to a lesser degree, the sagittal sinus. Only very little Pyr is detected in the brain. By contrast, while Lac is highest in the tongue, it also shows high signal throughout the whole brain.

Metabolic maps of Lac at eight time points from an animal after injection of HP [1-^{13}C]Lac are shown in Figure 6A. Signal from potential metabolic products Pyr, Ala, and bicarbonate (Bic) was below the detection threshold. The corresponding time series of Pyr and Lac maps of an animal

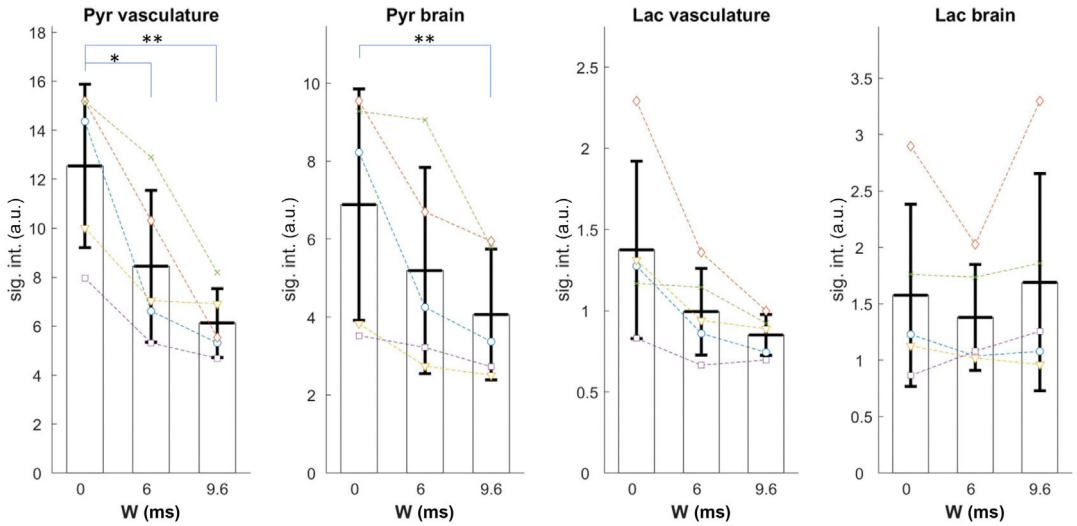

FIGURE 4 Mean and standard deviation ($n = 5$) of time-averaged Pyr and Lac in vascular and brain ROIs. Signal intensity (sig. int.) is normalized to the mean Ala intensity in muscle ROI for each imaging experiment. Data points for each individual subject are shown in dashed lines. Significant differences are found in vascular Pyr (W = 9.6 vs. W = 0 ms and W = 6 vs. W = 0 ms), as well as for brain Pyr (W = 9.6 vs. W = 0 ms). Neither differences in vascular nor brain Lac were statistically significant for any pair of W values. $^{*}p < 0.05$; $^{**}p < 0.01$ for correlated samples. Ala, alanine; Lac, lactate; Pyr, pyruvate; ROI, region of interest.

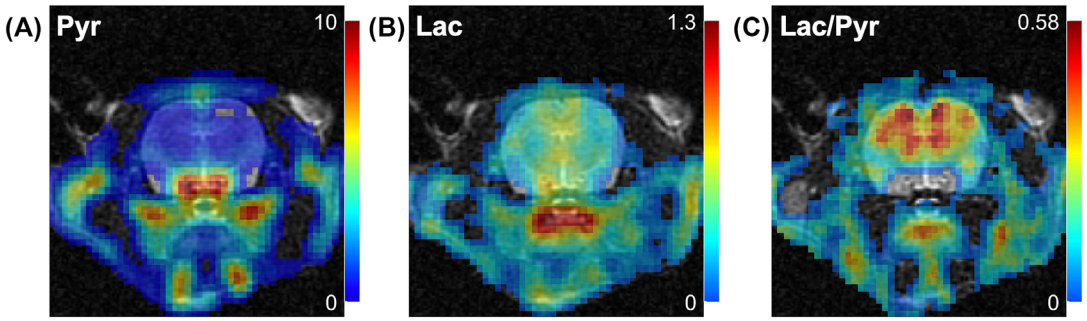

FIGURE 5 High-resolution 2D spCSI of healthy rat brain after a single [1-^{13}C]Pyr injection. Time-averaged metabolic maps of (A) Pyr (signal threshold 8%), (B) Lac (signal threshold 20%), and (C) Lac-to-Pyr ratio masked on an ROI with pyruvate intensity threshold of 12% and ratio threshold larger than 0.11. The highest Pyr signal was observed in the major vascular structures (Circle of Willis and sagittal sinus), whereas the high Lac signal was detected in the tongue muscle as well as in the brain. The high Lac/Pyr ratio throughout the brain provides more evidence that the lactate signal is from the brain itself rather than due to partial volume effects from major vessels. 2D spCSI, two-dimensional spiral chemical shift imaging; Lac, lactate; Pyr, pyruvate; ROI, region of interest.

after injection of HP [1-^{13}C]Pyr are shown in Figure 6B,C. The Lac maps acquired after injection of HP [1-^{13}C]Lac show similar distribution and dynamic patterns as the Pyr maps when [1-^{13}C]Pyr was used as the substrate. Signal of the respective substrate was highest in the vasculature and decayed quickly, with little signal appearing in the brain. By contrast, high signal of the product lactate was detected in the brain and its intensity remained high for several time frames.

4 | DISCUSSION

The presented data from the experiments with flow-sensitizing gradients demonstrate distinctively different signal behavior for Pyr and Lac in brain and vascular ROIs that cannot be caused by any systematic differences in the substrate concentration. Pyr in the vascular, as well as in the brain ROI, decreased with increase in flow suppression. The mean velocity of blood in the interior carotid arteries is of the order of 40 cm/s,[31–33] while in the capillaries it is lower by two orders of magnitude.[34,35] Assuming a laminar flow profile, the suppression factor for the gradients used in this study as a function of peak flow velocity is shown in Figure S3. Based on these estimates, metabolite signal in the arteries should be suppressed by approximately 80%, whereas in vessels with velocities of less than 1 cm/s the suppression is less than ~10%, even for the case of

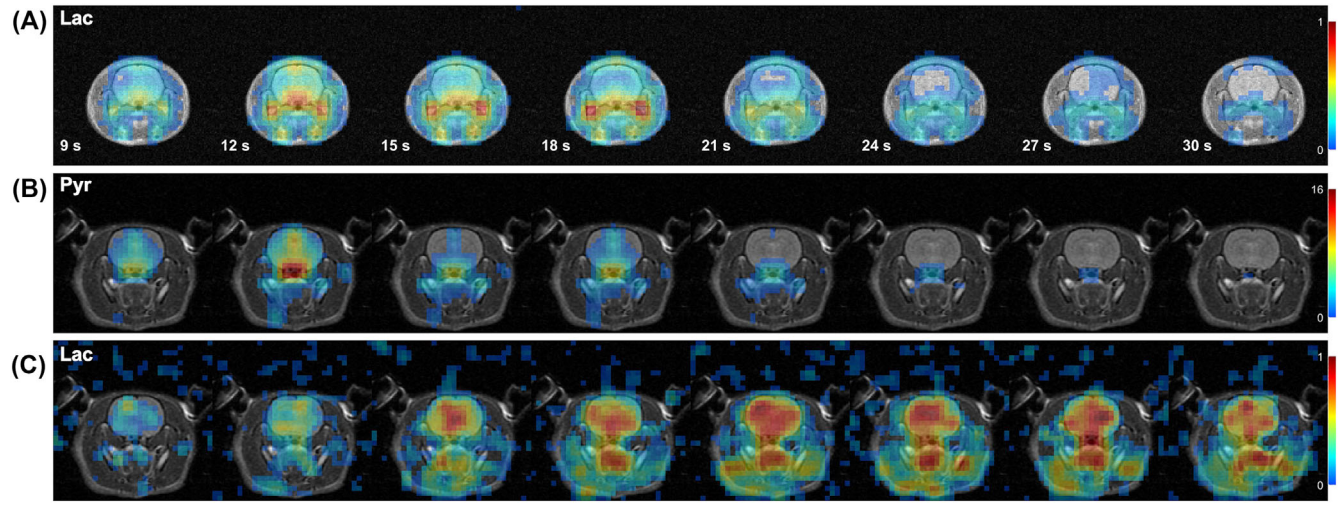

FIGURE 6 Metabolic maps from eight time points at 3-s temporal resolution for two healthy rats. (A) Lac maps from 3D spCSI for the animal with HP [1-^{13}C]Lac as substrate. (B) Pyr, and (C) Lac maps for an animal with HP [1-^{13}C]Pyr as substrate. In (A) and (B), the substrate signal was highest mostly in the vasculature at earlier time frames and then quickly decayed. In (C), the product lactate in brain appeared approximately 3 s after the arrival of substrate bolus, and its intensity remained high for several time frames. 3D spCSI, three-dimensional spiral chemical shift imaging; HP, hyperpolarized; Lac, lactate; Pyr, pyruvate.

W = 9.6 ms. The fact that brain Pyr was also affected by flow suppression was most likely predominantly due to partial volume effects from vascular signal because of the limited resolution, as discussed below in the comparison with the high-resolution data. However, it is also consistent with transport across the BBB being the rate-limiting step in the conversion of HP Pyr to Lac,[2] that is, any Pyr that has crossed the BBB is quickly converted to Lac, and Pyr signal detected in a brain ROI is predominantly from the blood pool, hence, more sensitive to flow-suppression gradients. By contrast, no change in brain Lac was detected with increasing levels of flow suppression. These results suggest that Lac and Pyr signals in the brain predominantly reside in different compartments, providing further evidence that the majority of the Lac in brain was a consequence of cerebral metabolism.

As was demonstrated by applications for cardiac and abdominal imaging, adding flow-sensitizing gradients to pulse sequences for brain imaging studies significantly reduces Pyr contributions from vascular compartments to the brain. Although there was no direct signal reduction for brain Lac due to flow effects, the additional gradients extended the minimum possible TE, hence, reducing Lac signal due to T2* decay and evolution of J-coupling. With an estimated effective T2* of ~30 ms, the addition of flow-sensitizing gradients led to a reduction of brain Lac of approximately 33% for W = 6 ms and 47% for W = 9.6 ms. Although the duration of the gradients can certainly be reduced when using dedicated animal scanners with stronger and faster gradient systems, the signal reduction due to extended TE needs to be taken into consideration when deciding whether flow suppression would overall be beneficial in preclinical studies of HP Pyr in the brain.

Comparison of the metabolic maps acquired at low and high in-plane resolution reveals significant partial volume effects for Pyr in the lower-resolution maps. High signal in vascular structures superior and posterior to the brain, which were better resolved in the high-resolution data, contributed to the signal in the brain ROI at lower resolution. At the same time, similar to the lower-resolution maps, Lac is detected throughout the whole brain, even at the higher resolution. Although Lac generated in organs such as the heart and liver is released into the circulation,[36–39] the high-resolution data suggest that vascular Lac is at about the same level as brain Lac and, hence, at the lower resolution it is not a large vascular component contributing to the lactate signal in the brain ROIs in the same way as is the case for Pyr.

When using Lac as the substrate its metabolic map and time course are similar to the low-resolution Pyr data, with the signal predominately in the vasculature. The lack of any signal of Pyr and its metabolic products Ala and Bic is consistent with the results of abdominal imaging of HP [1-^{13}C]Lac in healthy rats[40] because the conversion between Pyr and Lac is dominated by isotopic exchange.[41,42] As the physiological tissue concentration of Pyr is smaller than Lac by at least an order of magnitude,[43] the Pyr pool size is usually too small for significant exchange with the injected HP Lac, hence, Pyr and its metabolic products Ala and Bic were below the detection threshold.

Furthermore, at the concentration levels present in HP ^{13}C experiments, the transport across the BBB in adult rats is slower for Lac compared with Pyr. Considering both the active (saturable) and the passive diffusion (unsaturable) contributions to the transport, it has been shown that only at concentrations larger than approximately 35 mM, measured in the right carotid artery, does the transport rate across the BBB for lactate exceed that of pyruvate.[44] Therefore, it is rather unlikely that the Lac observed in the brain after Pyr injection was generated in other organs such as the heart and then transported across the BBB into the brain.

As substrate transport across the BBB is the rate-limiting step in brain pyruvate metabolism, higher conversion is indeed more likely "in diseases in which the blood brain barrier is expected to be focally disrupted", as posed by Miller et al.[19] Additionally, it has been shown in multiple

studies that the level and type of anesthesia and carrier gas affect the metabolic conversion in HP ^{13}C MRI/MRS.[4,45–48] Nevertheless, altogether the presented results provide further evidence that, even in healthy anesthetized rodents, the transport of HP Pyr across the BBB is sufficiently fast to permit detection of its metabolic conversion within the brain when using appropriate acquisition protocols. Therefore, we propose that metabolic imaging of HP pyruvate is a viable noninvasive tool for probing rodent brain pyruvate metabolism in preclinical studies.

ACKNOWLEDGMENTS

The authors thank Joshua Rogers, MEng, for his assistance in animal handling and monitoring. This work was supported by NIH grants R21 NS096575, R01 DK106395, R21 CA213020, R21 CA202694, R01 EB009070, R01 NS107409, and R21 GM137227. We also acknowledge the support of the University of Maryland, Baltimore, Institute for Clinical & Translational Research (ICTR) and Clinical Translational Science Award (CTSA) grant number 1UL1TR003098.

CONFLICT OF INTEREST STATEMENT

S.J. is an employee of Siemens Healthineers.

ORCID

Jae Mo Park https://orcid.org/0000-0002-7404-6971
Yi-Fen Yen https://orcid.org/0000-0001-9986-5327
Dirk Mayer https://orcid.org/0000-0001-7557-9019

REFERENCES

1. Hurd RE, Yen YF, Mayer D, et al. Metabolic imaging in the anesthetized rat brain using hyperpolarized [1-13C] pyruvate and [1-13C] ethyl pyruvate. *Magn Reson Med*. 2010;63(5):1137-1143. doi:10.1002/mrm.22364
2. Hurd RE, Yen YF, Tropp J, Pfefferbaum A, Spielman DM, Mayer D. Cerebral dynamics and metabolism of hyperpolarized [1-13C]pyruvate using time-resolved MR spectroscopic imaging. *J Cereb Blood Flow Metab*. 2010;30(10):1734-1741. doi:10.1038/jcbfm.2010.93
3. Mayer D, Yen YF, Takahashi A, et al. Dynamic and high-resolution metabolic imaging of hyperpolarized [1-13C]-pyruvate in the rat brain using a high-performance gradient insert. *Magn Reson Med*. 2011;65(5):1228-1233. doi:10.1002/mrm.22707
4. Josan S, Hurd R, Billingsley K, et al. Effects of isoflurane anesthesia on hyperpolarized 13C metabolic measurements in rat brain. *Magn Reson Med*. 2013;70(4):1117-1124. doi:10.1002/mrm.24532
5. Park JM, Josan S, Grafendorfer T, et al. Measuring mitochondrial metabolism in rat brain in vivo using MR spectroscopy of hyperpolarized [2-^{13}C]pyruvate. *NMR Biomed*. 2013;26(10):1197-1203. doi:10.1002/nbm.2935
6. Marjańska M, Iltis I, Shestov AA, et al. In vivo 13C spectroscopy in the rat brain using hyperpolarized [1-(13)C]pyruvate and [2-(13)C]pyruvate. *J Magn Reson*. 2010;206(2):210-218. doi:10.1016/j.jmr.2010.07.006
7. Park I, Larson PEZ, Zierhut ML, et al. Hyperpolarized 13C magnetic resonance metabolic imaging: application to brain tumors. *Neuro-Oncol*. 2010;12(2):133-144. doi:10.1093/neuonc/nop043
8. Day SE, Kettunen MI, Cherukuri MK, et al. Detecting response of rat C6 glioma tumors to radiotherapy using hyperpolarized [1-13C]pyruvate and 13C magnetic resonance spectroscopic imaging. *Magn Reson Med*. 2011;65(2):557-563. doi:10.1002/mrm.22698
9. Park JM, Josan S, Jang T, et al. Metabolite kinetics in C6 rat glioma model using magnetic resonance spectroscopic imaging of hyperpolarized [1-(13)C] pyruvate. *Magn Reson Med*. 2012;68(6):1886-1893. doi:10.1002/mrm.24181
10. Chaumeil MM, Ozawa T, Park I, et al. Hyperpolarized 13C MR spectroscopic imaging can be used to monitor Everolimus treatment in vivo in an orthotopic rodent model of glioblastoma. *Neuroimage*. 2012;59(1):193-201. doi:10.1016/j.neuroimage.2011.07.034
11. Park JM, Recht LD, Josan S, et al. Metabolic response of glioma to dichloroacetate measured in vivo by hyperpolarized (13)C magnetic resonance spectroscopic imaging. *Neuro-Oncol*. 2013;15(4):433-441. doi:10.1093/neuonc/nos319
12. Park JM, Spielman DM, Josan S, et al. Hyperpolarized (13)C-lactate to (13)C-bicarbonate ratio as a biomarker for monitoring the acute response of anti-vascular endothelial growth factor (anti-VEGF) treatment. *NMR Biomed*. 2016;29(5):650-659. doi:10.1002/nbm.3509
13. Guglielmetti C, Chou A, Krukowski K, et al. In vivo metabolic imaging of traumatic brain injury. *Sci Rep*. 2017;7:17525. doi:10.1038/s41598-017-17758-4
14. DeVience SJ, Lu X, Proctor J, et al. Metabolic imaging of energy metabolism in traumatic brain injury using hyperpolarized [1-(13)C]pyruvate. *Sci Rep*. 2017;7(1):1907. doi:10.1038/s41598-017-01736-x
15. Hackett EP, Chen J, Ingle L, et al. Longitudinal assessment of mitochondrial dysfunction in acute traumatic brain injury using hyperpolarized [1-13C] pyruvate. *Magn Reson Med*. 2023;90(6):2432-2442. doi:10.1002/mrm.29794
16. Guglielmetti C, Najac C, Didonna A, Van der Linden A, Ronen SM, Chaumeil MM. Hyperpolarized 13C MR metabolic imaging can detect neuroinflammation in vivo in a multiple sclerosis murine model. *Proc Natl Acad Sci*. 2017;114(33):E6982-E6991. doi:10.1073/pnas.1613345114
17. Le Page LM, Guglielmetti C, Najac CF, Tiret B, Chaumeil MM. Hyperpolarized 13C magnetic resonance spectroscopy detects toxin-induced neuroinflammation in mice. *NMR Biomed*. 2019;32(11):e4164. doi:10.1002/nbm.4164
18. Guglielmetti C, Cordano C, Najac C, Green AJ, Chaumeil MM. Imaging immunomodulatory treatment responses in a multiple sclerosis mouse model using hyperpolarized 13C metabolic MRI. *Commun Med*. 2023;3(1):71. doi:10.1038/s43856-023-00300-1
19. Miller JJ, Grist JT, Serres S, et al. 13C pyruvate transport across the blood-brain barrier in preclinical hyperpolarised MRI. *Sci Rep*. 2018;8(1):15082. doi:10.1038/s41598-018-33363-5
20. Ye FQ, Mattay VS, Jezzard P, Frank JA, Weinberger DR, McLaughlin AC. Correction for vascular artifacts in cerebral blood flow values measured by using arterial spin tagging techniques. *Magn Reson Med*. 1997;37(2):226-235. doi:10.1002/mrm.1910370215

21. Pell GS, Lewis DP, Branch CA. Pulsed arterial spin labeling using TurboFLASH with suppression of intravascular signal. *Magn Reson Med*. 2003;49(2):341-350. doi:10.1002/mrm.10373
22. Gordon JW, Niles DJ, Adamson EB, Johnson KM, Fain SB. Application of flow sensitive gradients for improved measures of metabolism using hyperpolarized 13C MRI. *Magn Reson Med*. 2016;75(3):1242-1248. doi:10.1002/mrm.25584
23. Lau AZ, Miller JJ, Robson MD, Tyler DJ. Cardiac perfusion imaging using hyperpolarized (13)C urea using flow sensitizing gradients. *Magn Reson Med*. 2016;75(4):1474-1483. doi:10.1002/mrm.25713
24. Lee H, Lee J, Joe E, et al. Flow-suppressed hyperpolarized 13C chemical shift imaging using velocity-optimized bipolar gradient in mouse liver tumors at 9.4 T. *Magn Reson Med*. 2017;78(5):1674-1682. doi:10.1002/mrm.26578
25. Mayer D, Yen YF, Josan S, et al. Application of hyperpolarized [1-^{13}C]lactate for the in vivo investigation of cardiac metabolism. *NMR Biomed*. 2012;25(10):1119-1124. doi:10.1002/nbm.2778
26. Mayer D, Yen YF, Tropp J, Pfefferbaum A, Hurd RE, Spielman DM. Application of subsecond spiral chemical shift imaging to real-time multislice metabolic imaging of the rat in vivo after injection of hyperpolarized 13C1-pyruvate. *Magn Reson Med*. 2009;62(3):557-564. doi:10.1002/mrm.22041
27. Lustig M, Kim S-J, Pauly JM. A fast method for designing time-optimal gradient waveforms for arbitrary k-space trajectories. *IEEE Trans Med Imaging*. 2008;27(6):866-873. doi:10.1109/TMI.2008.922699
28. Hargreaves BA, Nishimura DG, Conolly SM. Time-optimal multidimensional gradient waveform design for rapid imaging. *Magn Reson Med*. 2004;51(1):81-92. doi:10.1002/mrm.10666
29. Zhao L, Mulkern R, Tseng C, et al. Gradient-echo imaging considerations for hyperpolarized 129Xe MR. *J Magn Reson B*. 1996;113(2):179-183. doi:10.1006/jmrb.1996.0173
30. Josan S, Spielman D, Yen YF, Hurd R, Pfefferbaum A, Mayer D. Fast volumetric imaging of ethanol metabolism in rat liver with hyperpolarized [1-(13) C]pyruvate. *NMR Biomed*. 2012;25(8):993-999. doi:10.1002/nbm.2762
31. Lapergue B, Deroide N, Pocard M, Michel JB, Meilhac O, Bonnin P. Transcranial duplex sonography for monitoring circle of Willis artery occlusion in a rat embolic stroke model. *J Neurosci Methods*. 2011;197(2):289-296. doi:10.1016/j.jneumeth.2011.02.016
32. Larkin JR, Simard MA, Khrapitchev AA, et al. Quantitative blood flow measurement in rat brain with multiphase arterial spin labelling magnetic resonance imaging. *J Cereb Blood Flow Metab*. 2019;39(8):1557-1569. doi:10.1177/0271678X18756218
33. Wang Y, Zhang T, Zhang Y, et al. Effects of inverted photoperiods on the blood pressure and carotid artery of spontaneously hypertensive rats and Wistar–Kyoto rats. *J Hypertens*. 2021;39(5):871-879. doi:10.1097/HJH.0000000000002732
34. Ivanov KP, Kalinina MK, Levkovich YI. Blood flow velocity in capillaries of brain and muscles and its physiological significance. *Microvasc Res*. 1981;22(2):143-155. doi:10.1016/0026-2862(81)90084-4
35. Seylaz J, Charbonné R, Nanri K, et al. Dynamic in vivo measurement of erythrocyte velocity and flow in capillaries and of microvessel diameter in the rat brain by confocal laser microscopy. *J Cereb Blood Flow Metab*. 1999;19(8):863-870. doi:10.1097/00004647-199908000-00005
36. Chen AP, Leung K, Lam W, Hurd RE, Vigneron DB, Cunningham CH. Design of spectral-spatial outer volume suppression RF pulses for tissue specific metabolic characterization with hyperpolarized 13C pyruvate. *J Magn Reson*. 2009;200(2):344-348. doi:10.1016/j.jmr.2009.06.021
37. Xu T, Mayer D, Gu M, et al. Quantification of in vivo metabolic kinetics of hyperpolarized pyruvate in rat kidneys using dynamic 13C MRSI. *NMR Biomed*. 2011;24(8):997-1005. doi:10.1002/nbm.1719
38. Marjańska M, Teisseyre TZ. Measurement of arterial input function in hyperpolarized 13C studies. *Appl Magn Reson*. 2012;43:289-297. doi:10.1007/s00723-012-0348-3
39. Wespi P, Steinhauser J, Kwiatkowski G, Kozerke S. Overestimation of cardiac lactate production caused by liver metabolism of hyperpolarized [1-13C]pyruvate. *Magn Reson Med*. 2018;80(5):1882-1890. doi:10.1002/mrm.27197
40. Hurd RE, Spielman D, Josan S, Yen YF, Pfefferbaum A, Mayer D. Exchange-linked dissolution agents in dissolution-DNP 13C metabolic imaging. *Magn Reson Med*. 2013;70(4):936-942. doi:10.1002/mrm.24544
41. Day SE, Kettunen MI, Gallagher FA, et al. Detecting tumor response to treatment using hyperpolarized 13C magnetic resonance imaging and spectroscopy. *Nat Med*. 2007;13(11):1382-1387. doi:10.1038/nm1650
42. Witney TH, Kettunen MI, Brindle KM. Kinetic modeling of hyperpolarized 13C label exchange between pyruvate and lactate in tumor cells. *J Biol Chem*. 2011;286(28):24572-24580. doi:10.1074/jbc.M111.237727
43. Brooks GA. Lactate as a fulcrum of metabolism. *Redox Biol*. 2020;35:101454. doi:10.1016/j.redox.2020.101454
44. Cremer JE, Cunningham VJ, Pardridge WM, Braun LD, Oldendorf WH. Kinetics of blood-brain barrier transport of pyruvate, lactate and glucose in suckling, weanling and adult rats. *J Neurochem*. 1979;33(2):439-445. doi:10.1111/j.1471-4159.1979.tb05173.x
45. Marjańska M, Shestov AA, Deelchand DK, Kittelson E, Henry PG. Brain metabolism under different anesthetic conditions using hyperpolarized [1-13C]pyruvate and [2-13C]pyruvate. *NMR Biomed*. 2018;31(12):e4012. doi:10.1002/nbm.4012
46. Flatt E, Lanz B, Pilloud Y, et al. Measuring glycolytic activity with hyperpolarized [2H7, U-13C6] D-glucose in the naive mouse brain under different anesthetic conditions. *Metabolites*. 2021;11(7):413. doi:10.3390/metabo11070413
47. Hyppönen V, Stenroos P, Nivajärvi R, et al. Metabolism of hyperpolarised [1–13C]pyruvate in awake and anaesthetised rat brains. *NMR Biomed*. 2022;35(2):e4635. doi:10.1002/nbm.4635
48. Healicon R, Rooney CHE, Ball V, et al. Assessing the effect of anesthetic gas mixtures on hyperpolarized 13C pyruvate metabolism in the rat brain. *Magn Reson Med*. 2022;88(3):1324-1332. doi:10.1002/mrm.29274

SUPPORTING INFORMATION

Additional supporting information can be found online in the Supporting Information section at the end of this article.

How to cite this article: Zhu M, Jhajharia A, Josan S, et al. Investigating the origin of the ^{13}C lactate signal in the anesthetized healthy rat brain in vivo after hyperpolarized [1-^{13}C]pyruvate injection. *NMR in Biomedicine*. 2024;37(3):e5073. doi:10.1002/nbm.5073